444 KSME Journal, Vol. 8, No. 4, pp. 444~459, 1994

# Experiments on the Turbulent Shear Flow in a Turn-Around Duct(I) — The Mean Flow Characteristics

**Jung-Chul Shin***

(*Received March 16, 1994*)

The Complex turbulent water flow in a strongly curved turn-around duct has been studied. The turn-around duct had an aspect ratio of 10 : 1 and the ratio of the channel height to the mean radius was 1.0. Extensive measurements throughout the curved duct including wall static pressures and mean velocities were made using Laser Doppler Velocimeter for a Reynolds number of 210,000 based on the height of the channel and the average velocity. Analytical calculations of the potential flow were made using Green's function and the Rayleigh-Ritz method. Based on the turbulence mechanism and stability consideration, a simplified physical model for the outer layer near the start of the turn along the inner convex wall was hypothesized. This physical model leads to a system of non-linear equations represented in orthogonal curvilinear coordinates. These equations were solved numerically using an iteration method. Comparison of the measured data with the calculated values reveals that the present flow shows the characteristics of an inertial dominated, developing curved flow. The outer layer in a quasi-laminar flow was governed by inviscid-rotational motion. The numerical solution for this region was verified by comparing the calculated and measured flow results. Near the turn exit along the inner wall, a large flow reversal was observed. Spanwise measurements showed that the present turn-around duct flow was approximately two-dimensional. The local mean velocity profiles in the turn for different flow rates were similar when normalized by the average velocity.

**Key Words :** Turbulent Shear Flow, Laser Doppler Velocimeter, Highly Curved Duct Flow, Boundary Layer Parameters, Wall Static Pressure, Curved Potential Flow, Inviscid-Rotational Flow, Surface Shear Stress

## 1. Introduction

Turbulent shear flow in a turn-around duct is a problem which may be found in a number of flow fields, such as rocket engines or nuclear reactors which have complex flow passages. By understanding the complex turbulent shear flow in a curved channel, it may be possible to investigate the flow structure inside a reactor core as well as other flow passages in the reactor coolant system. Compact design for high thrust-to-weight ratio, liquid rocket engines demands highly curved flow paths. The present turn-around duct flow is a simplified model for simulation of the flow passage downstream of the turbine in the fuel preburner inside the Space Shuttle Main Engine.

Only limited studies, experimental and/or numerical, for strongly curved two-dimensional channel flows in which different flow structures are combined, have been attempted. Curved channel flow may be divided into two categories ; the shear dominated, mildly curved flow and the inertia dominated, strongly curved flow. The flow characteristics are different for the two cases. (Hunt et al., 1979)

The boundary layer on a curved surface is stable along a convex wall and unstable along a concave wall according to Rayleigh's instability criteria(Rayleigh, 1917). Turbulent fluctuations decrease along the convex wall and increase along the concave wall. Accordingly the boundary layer

* Korea Atomic Energy Research Institute

growth is slower over convex surfaces and faster over concave surfaces. Along the inner convex wall the present flow is influenced by both a strong favorable pressure gradient and the curvature, which produce a laminarization near the start of the turn. For the present flow the streamwise distance is too short to reach a complete laminar state and therefore a quasi-laminar state is more plausible. Although there were several earlier investigators about laminarization, Launder(1963) was the first to report in detail about the laminarization. His verification of the laminarization was obtained by observing the departure from universality of the law of the wall. A pressure gradient was imposed on a flat test plate by a two-dimensional nozzle. Badrinarayanan and Ramjee(1969) observed the laminarization from the reduction of the streamwise fluctuations normalized by the free stream velocity in the acceleration region. The instability along the outer concave wall for the turbulent flows can generate Taylor-Görtler vortices which wander from side to side due to ; the turbulence in the shear layer, the large scale turbulence or the non-uniformity in the incoming flow. Some investigators(Hunt et al., 1979; So et al., 1972; MerDney et al., 1972) reported stationary patterns of Taylor-Görtler vortices while others(Eskinazi et al., 1956; Ellis et al., 1974; Ramaprian et al., 1978; Barlow et al., 1988) have no evidence of such structures. Patel, et al.(1968) demonstrated that the boundary layer on a convex wall was relatively two-dimensional near the center line for the first 80° of the bend. So and Mellor(1972) measured a turbulent boundary layer developed over a flat surface and then passed to convex and concave surfaces which were adjustable to produce either a constant or an adverse pressure gradient. The mean velocity calculation was made using Bernoulli's equation and by assuming $\partial P/\partial y = \rho k U^2$, where $k$ is the curvature of the inner wall, $k = 1/R$. The boundary layer thickness changed very little over the curved region. For the constant pressure gradient flow, the local skin friction coefficient, $C_f$ was smaller on the convex wall and larger on the concave wall when compared to the plane wall. Similar variations of skin friction on curved surface were reported by others(Meroney et al., 1975; Gillis et al., 1983; Muck et al., 1985). The log-law velocity distribution for fully developed curved duct flow was valid only in a limited region, $y^+ \leq 200$, which agrees with measurements of Eskinazi and Yeh(1956).

Although some results were reported previously for the curved channel flow (Wattendorf, 1935; Wilken, 1930), the detailed experimental investigation in a strongly curved duct flow has not yet been reported. While the present experimental investigations cover the region throughout the curved duct, this study emphasizes the quasi-laminar region. The surface shear stress variation with Reynolds number was measured along the concave wall.

## 2. Experimental Works

A special two-dimensional turn-around duct model was constructed for the present study as shown in Fig. 1. The side walls of the test section were made of 2.54 cm thick lucite so that the Laser doppler velocimeter could be operated. Lake water from a large reservoir located above the test facility comes directly into the test section of the U-turn facility. The density and viscosity of the test water were measured with a hydrometer and a Ostwald type viscometer. The density and viscosity were found not to be different from the tabulated data. The flow rate was controlled by a 0.61 m control valve located about 95 m upstream from the entrance of the test section. The coordinate system used in the analysis is a curvilinear coordinate system attached on the inner convex wall as seen in Fig. 2. A Laser Doppler Velocimeter(LDV) was employed to measure the velocity field. A He-Ne Laser is used as the LDV light source. In the present study, the forward scatter, dual beam optical system was employed. A 19 mW He-Ne Laser was used in conjuction with a counter-type signal processor. The counter measures the time duration for a given number of doppler burst cycles and allows the evaluation of frequencies for discontinuous, unrelated burst signals. The counter makes it possible to accurate-

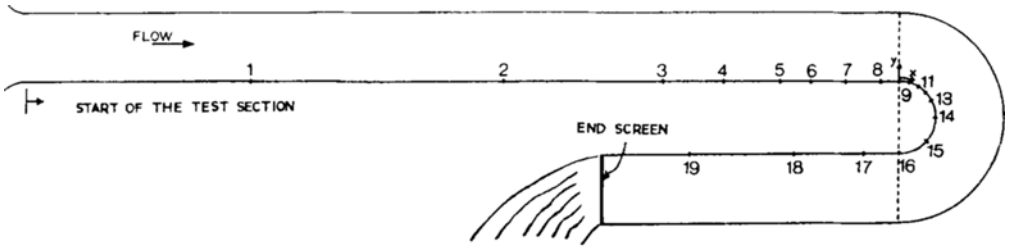


| STATION NO. | START | 1 | 2 | 3 | 4 | 5 | 6 | 7 | 8 | 9 | 10 | 11 | 12 |
|---|---|---|---|---|---|---|---|---|---|---|---|---|---|
| X ( Cm ) | -127.0 | -94.0 | -57.2 | -34.3 | -25.4 | -17.3 | -12.7 | -7.62 | -2.54 | 0.0 | 1.31 | 2.62 | 3.93 |
| DEGREE | | | | | | | | | | | 15° | 30° | 45° |

| 13 | 14 | 15 | 16 | 17 | 18 | 19 | END |
|---|---|---|---|---|---|---|---|
| 5.24 | 7.90 | 10.5 | 15.7 | 20.8 | 30.9 | 42.4 | 58.9 |
| 60° | 90° | 120° | 180° | | | | |

**Fig. 1** Measuring stations along the curved channel

ly measure the flow velocity in a situation where the concentration of seeding particles is relatively low. A frequency shifter was utilized to measure the mean velocity inside the separation bubble ; it allows measurements to be made in a reversed flow by shifting the doppler frequency at zero velocity. A Bragg Cell installed in the transmitting side shifts the light frequency. A band-pass filter(3 MHz low-pass filter and 30 KHz high-pass filter) was used to reduce the noise of the signal and retain the energy containing frequency range of the flow. Two-component velocity measurement were made by rotating the two incident beams by $\pm 45°$ from the plane parallel to the wall. A sine wave from an oscillator was used to calibrate the counter. A detailed set of measurements were made emphasizing the quasi-laminar region near the start of the inner convex wall. The flow rate was maintained to yield the mean velocity of $U_m \simeq 2.82$ m/s ($Re \simeq 210{,}000$). Static taps were located, both on the inner and outer walls, at selected location along the centerline of the channel. Diaphragm, inductance type, pressure transducers were employed to convert the pressure difference to output voltage. The static pressure transducers were calibrated using a water manometer. A Stanton tube was used to measure the surface shear stress. The Stanton tube senses the mean flow velocity very near the surface. It was calibrated at the location $x/h = -1.73$ with the local surface shear determined using a Clauser's fitting of the mean velocity profiles.

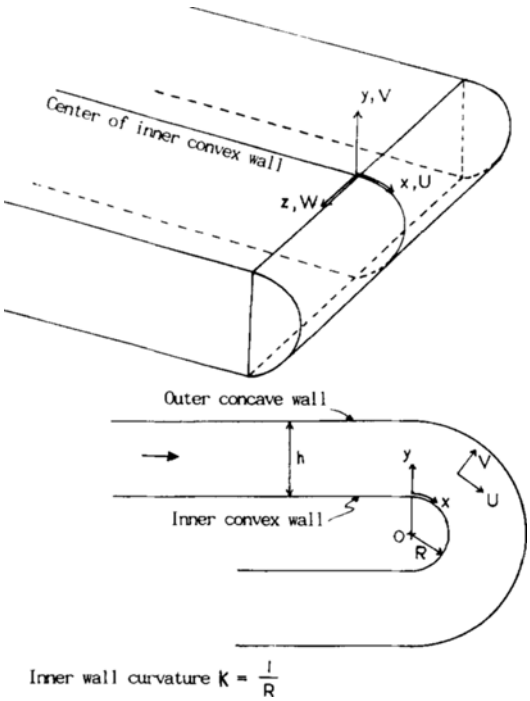


**Fig. 2** Coordinate system and notation for the analysis of the curved channel flow

## 3. Flow in a Turn-Around Duct

The time averaged equations for steady, two-

dimensional turbulent flow are as follows;

continuity;

$$\frac{\partial U}{\partial x}+\frac{\partial}{\partial y}\{(1+ky)V\}=0 \tag{1}$$

$x$-momentum;

$$\frac{1}{1+ky}U\frac{\partial U}{\partial x}+V\frac{\partial U}{\partial y}+\frac{k}{1+ky}UV$$
$$=-\frac{1}{\rho}\left[\frac{1}{1+ky}\frac{\partial P}{\partial x}+\frac{1}{1+ky}\frac{\partial}{\partial x}(-\rho u^2+\Pi_{xx})\right.$$
$$\left.+\frac{\partial}{\partial y}(-\rho uv+\Pi_{xy})+\frac{2k}{1+ky}(-\rho uv+\Pi_{xy})\right] \tag{2}$$

$y$-momentum;

$$\frac{1}{1+ky}U\frac{\partial V}{\partial x}+V\frac{\partial V}{\partial y}-\frac{k}{1+ky}U^2$$
$$=-\frac{1}{\rho}\left[\frac{\partial P}{\partial y}+\frac{1}{1+ky}\frac{\partial}{\partial x}(-\rho uv+\Pi_{xy})\right.$$
$$+\frac{\partial}{\partial y}(-\rho v^2+\Pi_{yy})-\frac{k}{1+ky}$$
$$\left.\{(-\rho u^2+\Pi_{xx})-(-\rho v^2+\Pi_{yy})\}\right] \tag{3}$$

where $\Pi$ is the viscous stress tensor. The present measurements indicated that the flow in a turn-around duct is approximately two-dimensional as seen in later. The global characteristics of the flow in a turn-around duct are noted on Fig. 3. The sudden appearance of a bend connected to the straight duct upstream produces a positive $\partial P/\partial y$ in the flow field in order to balance the centrifugal force caused by the streamline curvature. Near the start of the turn, therefore, the velocity must accelerate along the inner convex wall and decelerate along the outer concave wall in order to satisfy both the continuity condition across the two-dimensional curved duct with constant height and the Bernoulli's equation, if the second order viscous and turbulent effects are ignored. Consequently, an adverse streamwise pressure gradient develops along the outer wall and a favorable streamwise pressure gradient is formed along the inner wall near the start of the turn. The present measurements indicated that the incoming turbulent boundary layers along the inner and outer walls interacted in the turn before approximately the 90° station. Therefore the flow in the upstream part of the turn is developing toward a fully developed curved duct flow. Due to the inertial effect, the flow in the downstream part of the turn is directed toward the outer wall as seen in Fig. 4 in which $\psi'$ is a normalized stream function. Along the concave wall the higher momentum fluid moves toward the wall and thus surface shear becomes greater. Along the convex wall the higher momentum fluid moves away from the wall and therefore lower surface shear is encountered. After approximately 90° around the turn the present flow approaches the characteristics of an inertial dominated, fully developed, curved duct flow.

Near the turn exit along the inner wall the higher momentum fluid moves away from the wall due to the inertial effect. In addition an adverse streamwise pressure gradient develops along the inner wall, since the static pressure across the duct tends to be uniform in order to recover to the flat wall flow in the straight duct flow downstream, according to the potential flow

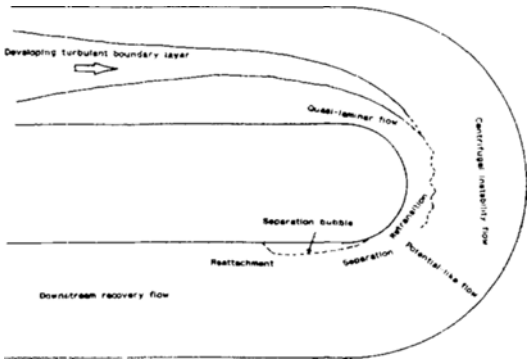


**Fig. 3** Global characteristics of the flow in a turn-around duct

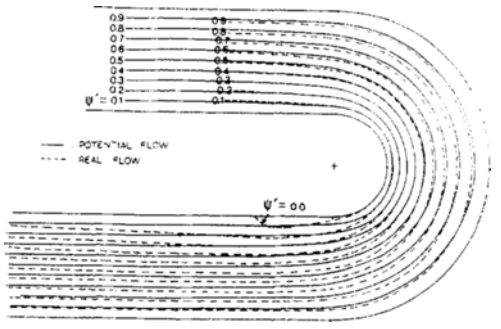


**Fig. 4** Streamlines along the turn-around duct flow. Re=86,000

analysis. Consequently the sharp curvature and strong adverse pressure gradient cause the boundary layer to separate. The flow reverses and forms a separation bubble along the inner wall at the turn exit. In an inertial dominated, strongly curved duct flow a distinct potential flow region exists across the duct, skewed toward the outer wall, when it is fully developed (Eskinazi et al., 1956; Ellis et al., 1974; Wattendorf, 1935). The present flow in the downstream part of the turn was in close agreement with the potential flow analysis results except near the wall as seen in Fig. 4. In the Taylor-Görtler vortices, inflows and outflows occur alternatively along the spanwise direction. At the inflow, the flow directions are towards the wall. Therefore, the boundary layer becomes thinner and the skin friction coefficient, $C_f$ becomes greater at the inflow, because higher momentum fluid moves toward the wall. For the outflow, the flow directions are away from the wall and the boundary layer becomes thicker. Consequently, $C_f$ has the smallest value at the outflow locations.

## 4. Analytical Evaluation of the Potential Flow Field

The potential flow solution is necessary to investigate the mean flow characteristics. The general solution for the potential flow field for various turning angles and heights of bends with constant radius was obtained analytically. A computer program was developed using the method of LU decomposition(Press et al., 1986) and Simpson's integral rule so that it can be used for the calculation of flow in bends in conjunction with straight channels.

The stream function, $\psi$, in an incompressible, two-dimensional potential flow satisfies the Laplace equation,

$$\nabla^2\psi=0 \tag{4}$$

In order to solve the Laplace equation in a bend, the bend with arbitrary turning angle, $2\varphi\pi$(rad), is divided into two parts as shown in Fig. 5. It is convenient to use the cartesian coordinate system in the straight section and the cylindrical coordinate system in the curved section. The static pressure coefficient $C_p=(P-P_\infty)/(1/2\,\rho U_m^2)$ (where $P_\infty$ is the static pressure far upstream from the bend) at any point in the irrotational flow field can be obtained from the Bernoulli's equation.

The solution of the elliptic equation, Eq. (4), is determined by the boundary conditions given on the surface of the physical domain. By simplifying the boundary conditions and matching the boundary condition at the junction between the straight section and the bend, the stream function in the straight section becomes,

$$\psi(x,\,y)=\frac{y}{h}+\sum_{n=1}^{\infty}a_n e^{\frac{n\pi x}{h}}\sin\frac{n\pi y}{h} \tag{5}$$

In the cylindrical section, a new variable, $Z$, is introduced.

$$Z=\psi-g \tag{6}$$

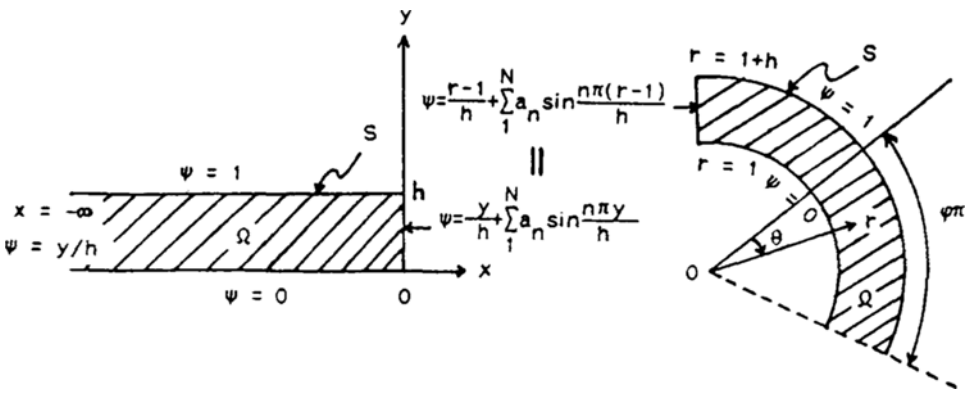


**Fig. 5** Boundary conditions in physical domain of a bend

Then Eq. (6) becomes the Poisson's equation.

$$\nabla^2 Z = -\nabla^2 g \quad (-\varphi\pi < \theta < \varphi\pi,\ 1 < r < 1+h)$$
$$Z = 0 \text{ on } S \tag{7}$$

where

$$g(r) = \frac{r-1}{h} + \sum_n a_n \sin\frac{n\pi(r-1)}{h}$$

It is well known that the Poisson's equation can be solved by means of Green's function. For constructing the Green's function in the given physical domain, the eigenfunction expansion method is introduced. The eigenfunctions for the Laplacian $\nabla^2$ in $\Omega$ subject to zero Dirichlet boundary conditions, are the non-zero solutions of the following equation,

$$\nabla^2 Z = \lambda Z \text{ in } \Omega$$
$$Z = 0 \quad \text{on } S \tag{8}$$

The Green's function in this region becomes,

$$G(r, \theta; r_0, \theta_0) = \sum_{m,n=1}^{\infty} \frac{Z_{mn}(r, \theta) Z_{mn}(r_0, \theta_0)}{\lambda_{mn}} \tag{9}$$

where $\lambda_{mn}$ and $Z_{mn}$ are the eigenvalues and the normalized eigenfunctions of Eq. (8) respectively. In order to obtain the eigenvalues and eigenfunctions in the curved section, a conformal mapping method is introduced. In conclusion, the stream function in the curved section is given by,

$$\psi(r, \theta) = \sum_{m=1}^{\infty}\sum_{n=1}^{\infty}(f_{mn} - g_{mn}\sum_k a_k \beta_{kn}) \sin(A_n \ln r)\cos(B_m\theta) + \frac{r-1}{h} + \sum_k a_k \sin\{C_k(r-1)\} \tag{10}$$

where,

$$A_n = \frac{n\pi}{\ln(1+h)},\quad B_m = \frac{2m-1}{2\varphi},\quad C_k = \frac{k\pi}{h}$$

$$f_{mn} = \frac{\frac{8}{n\pi^2}A_n^2\frac{(-1)^{m+1}}{2m-1}\left\{\frac{1}{h} - (-1)^n\left(1+\frac{1}{h}\right)\frac{1}{1-A_n^2}\right\}}{A_n^2 + B_m^2}$$

$$g_{mn} = \frac{\frac{8}{n\pi^2}A_n^2\frac{(-1)^{m+1}}{2m-1}}{A_n^2 + B_m^2}$$

$$\beta_{kn} = A_n\int_1^{1+h}\sin\{C_k(r-1)\}\sin(A_n\ln r)\frac{dr}{r} \tag{11}$$

The solution can be obtained if the coefficients 'a' appearing in Eqs. (5) and (10) are known. Lau(1966) introduced the Rayleigh-Ritz method to find the coefficients in the series solution. Mathematically, the Rayleigh-Ritz method requires that the following integral is a minimum if $\psi$ satisfies the Laplace equation.

$$I = \iint_{\text{whole area}} |\nabla\psi|^2 dA \tag{12}$$

where $dA$ is an area element. Eq. (12) implies that the kinetic energy in the area through the curved bend is a minimum. Therefore the relation,

$$\int_{-\infty}^{0}\int_0^h \frac{\partial}{\partial a_i}\left[\left(\frac{\partial\psi}{\partial x}\right)^2 + \left(\frac{\partial\psi}{\partial y}\right)^2\right]dydx + \frac{1}{2}\int_1^{1+h}\int_{-\varphi\pi}^{\varphi\pi}\frac{\partial}{\partial a_i}\left[\left(\frac{\partial\psi}{\partial r}\right)^2 + \left(\frac{\partial\varphi}{r\partial\theta}\right)^2\right]rd\theta dr = 0 \tag{13}$$

is satisfied. After much algebra the following linear algebraic equation for the coefficients $a_i$ is obtained.

$$\left[2i\pi + \frac{i^2\pi^3\varphi(h+2)}{h}\right]a_i + \sum_{k'\neq i}2\varphi i\pi k'\left[\frac{(-1)^{i-k'}-1}{(i+k')^2} + \frac{(-1)^{i-k'}-1}{(i-k')^2}\right]a_{k'} - \frac{64\varphi\pi}{[h\ln(1+h)]^3}\sum_k\left[\sum_m\sum_n \frac{\frac{n^2}{(2m-1)^2}\beta_{kn}\beta_{in}}{\left[\frac{n\pi}{h\ln(1+h)}\right]^2 - \left(\frac{2m-1}{2\varphi}\right)^2}\right]a_k = -\frac{64\varphi\pi}{h[h\ln(1+h)]^3}\sum_m\sum_n \frac{\frac{n^2}{(2m-1)^2}\frac{(-1)^n(1+h)-1}{1+\left[\frac{n\pi}{h\ln(1+h)}\right]^2}}{\left[\frac{n\pi}{h\ln(1+h)}\right]^2 + \left(\frac{2m-1}{2\varphi}\right)^2}\beta_{in} + \frac{4\varphi}{i}\{1-(-1)^i\} \tag{14}$$

where $i = 1, 2, 3, \cdots, N$.

Equation (14) has the following form,

$$\underline{B}\cdot\underline{a} = \underline{C} \tag{15}$$

where $\underline{B}$ is the coefficient matrix and $\underline{a}$ and $\underline{C}$ are column vectors. A system of algebraic linear equations for $\underline{a}$ was solved by the method of LU decomposition.

## 5. Numerical Calculation of the Rotational Flow Field

The viscous effect and turbulent fluctuations in the outer region of the boundary layer along a convex wall may be ignored in the present turn-around duct flow. It was found from the experimental results that the pressure force term dominates on the right-hand sides of the momentum Eqs. (2) and (3)(three orders of magnitude larger than the turbulent stress term). Therefore, the following momentum equations was hypothesized in the outer region.

$$U\frac{\partial U}{\partial x}+(1+ky)V\frac{\partial U}{\partial y}+kUV = -\frac{1}{\rho}\frac{\partial P}{\partial x} \tag{16}$$

$$U\frac{\partial V}{\partial x}+(1+ky)V\frac{\partial V}{\partial y}-kU^2 = -(1+ky)\frac{1}{\rho}\frac{\partial P}{\partial y} \tag{17}$$

which are the equations of motion for an inviscid but rotational flow in the curvilinear coordinate system.

A discretization equation was developed in order to solve this system of equations numerically in the curvilinear coordinate for incompressible, two-dimensional flow. The solution procedure was revised from Patankar's(1980) SIMPLER procedure using an elliptic pressure field sweeping from downstream to upstream. If the pressure is constant across the stream, a parabolic numerical scheme can be applied. The pressure varies along the normal direction in the present flow, such that the flow shows a partially parabolic behavior, since an elliptic numerical scheme was used for the pressure field. Therefore, the solution is obtained by marching the velocity field from the upstream to the downstream, while the downstream effects are transmitted to the upstream by the elliptic pressure field.

The boundary conditions were taken from the present experimental results. The physical domain contains from the upstream straight section to the 90° around the turn. The numerical grid($99\times 50$) in the computational domain was composed of an equally spaced rectangle with x and y increments. Since the wall curvature changes abruptly from zero to a finite value in the present flow, the under-relaxation was necessary. Relaxation of the quantity $\Phi$ is

$$\Phi=\zeta\Phi_{new}+(1-\zeta)\Phi_{old} \tag{18}$$

in which $\zeta$ is the relaxation factor. Velocities and pressures were underrelaxed with $\zeta=0.9$ during the iteration process. It was observed from the convergence history that 20~40 iteration is enough to obtain the converged solution with an error of less than 0.005% between the last two iterations.

## 6. Results and Discussion

### 6.1 Potential flow field

The comparison between the static pressure distributions at the wall obtained from the potential flow calculation and the measured data is shown in Fig. 6. The static pressure profiles as well as the potential velocity start to respond to the curvature approximately one duct height before the start and after the turn. The higher pressures than the measured ones around the turn except the separated region are expected because the potential flow calculations can not account for the energy loss through the turn. Along the inner wall near the start of the turn, the two distributions are nearly the same since the turbulence was damped due both to flow acceleration and to stabilizing convex curvature. The static pressure of the real flow on the outer wall does not vary greatly around the bend while on the inner wall the pressure drops rapidly at the start of the bend and then rises. At the inlet of the curved section an adverse streamwise pressure gradient develops along the outer wall and a favorable pressure gradient is formed along the inner surface. The inward normal pressure gradient exists across the channel section due to curvature, higher static pressure on the outer wall and lower on the inner wall. At about 180° the static pressure distributions on the outer wall becomes favorable, whereas an adverse pressure gradient is formed on the inner wall at about 90°. It is

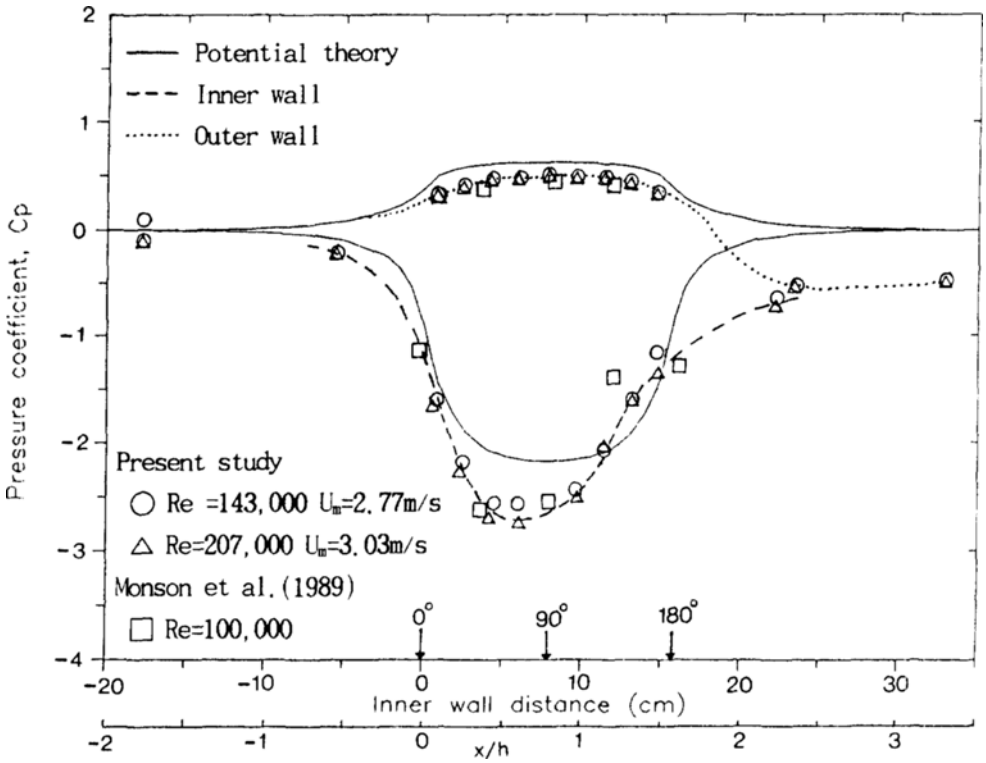


**Fig. 6** Static pressure distributions at the wall

observed that the measured wall static pressures in some portion along the inner convex wall after 90° is greater than predicted by the calculated potential flow. This higher $C_p$ is due to the inertial effect of the flow which causes lower momentum fluid near the wall, so that the static pressure rises. A comparison between the present study and Monson and Seegmiller(1989) who conducted a similar experiment in an air flow facility shows good agreement in Fig. 6.

Figures 7, 8, 9 show measured mean velocity profiles compared to the calculated potential velocities. Figure 7 shows that the potential core region exists for the flow upstream near the onset of curvature. The actual flow near the convex wall approaches the potential flow results around to the 90° Station due to the streamwise favorable pressure gradient. The actual flow near the concave wall in the downstream part of the turn tends to be close to the potential flow as the flow continues. This result indicates that the flow in the turn approaches the fully developed condition for curved duct flow. Accordingly the potential core region tends to be skewed toward the outer wall, downstream of the 90° Station. Therefore the potential core region around the curved section moves from the inner wall toward the outer wall, which is the characteristic of inertial dominated, developing curved flow. The calculated potential flow at 90° Station is found to be the same as the free vortex flow($U \cdot r$=constant where r is the radial distance from the axis of the curvature, $r = R + y$). This agreement indicates that the present calculations for the potential flow are reasonable. Beyond the 60° Station the mean velocity decreases and turbulent boundary layer separation eventually occurs on the inner convex wall. Due to the inertial effect and the adverse streamwise pressure gradient increasing in that region, the lower momentum fluid near the wall is encountered. The fluid in the boundary layer does not possess sufficient mean kinetic energy and

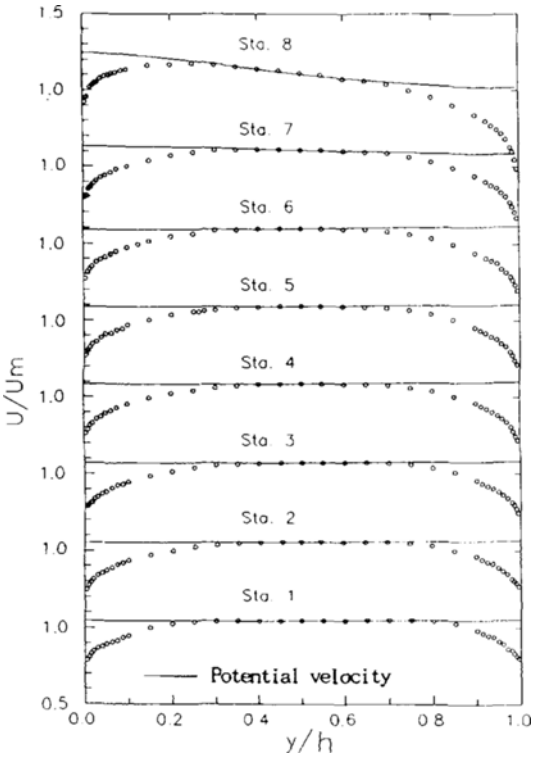


**Fig. 7** Mean velocity profiles along the approach duct upstream of the turn

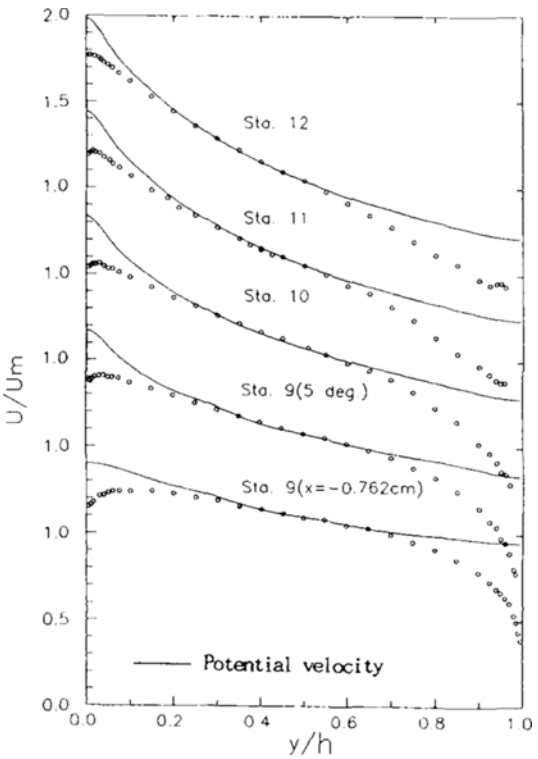


**Fig. 8** Mean velocity profiles near the start of the turn

finally separates at approximately 165° around the turn and reattachment occurs at approximately 0.74 h downstream from the turn exit. Figures 10, 11 show the flow angle variations around the curved duct. The measured flow angles are reasonably predicted by the potential flow calculations up to the 30° Station. Due to the inertial effect, the actual flow is directed toward the inner wall until 45° around the turn and then is directed away from the inner convex wall.

### 6.2 Rotational flow field

The computed results for the streamwise velocity at several locations along the streamwise direction are compared with the experimental data in Fig. 12. The results of the potential flow calculations are also included for comparison. The measured velocity data in the center regions are very close to the calculated inviscid flow, both rotational and irrotational, which indicates that the effect of the turbulent shear stress as well as the viscous shear stress can be neglected in the outer region of boundary layer. These results are consistent with the observation that the turbulence in the convex curvature region is almost extinguished. The close agreement between the calculated rotational and irrotational flows at 45 ° around the turn indicates that the present calculations for both flows are reasonable. The agreement between the measured data and the calculated values justifies that the present assumption for the rapid suppression of the turbulent shear stress along the inner convex wall is reasonable. However the region very near the wall is influenced by the viscous effect, which are not included in the present inviscid calculation. As expected, the rotational flow predicts the actual flow better than the potential flow. In other words, the flow has a certain amount of vorticity. The rotational flow calculations improve the irrotational predictions in the curved section where the maximum streamwise pressure gradient occurs. An insight into the quasi-laminar flow region can be

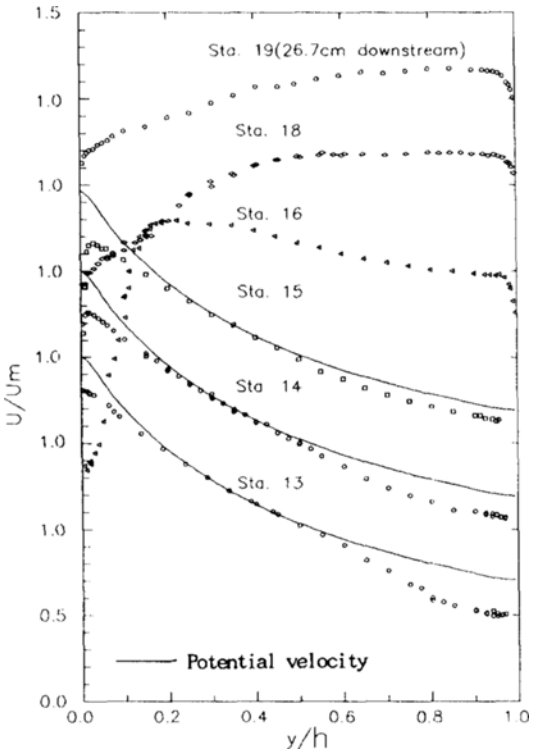


**Fig. 9** Mean velocity profiles in the turn and downstream of the turn

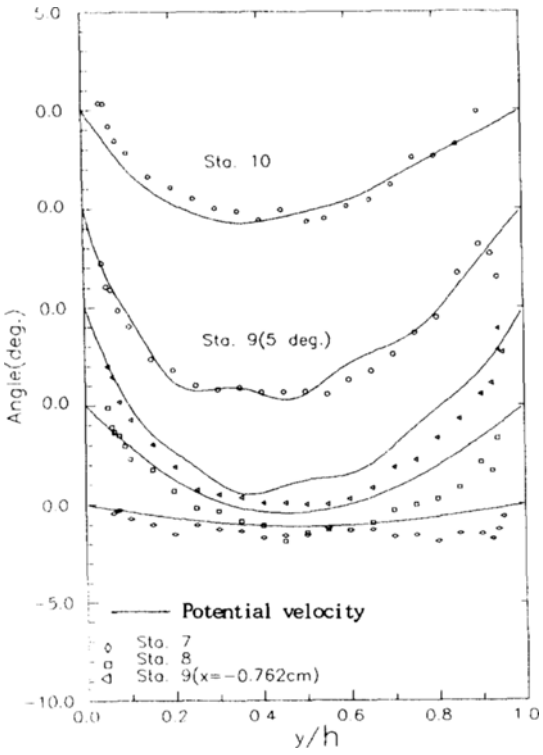


**Fig. 10** Flow angle profiles near the start of the turn

obtained by observing the behavior of vorticity along a streamline. Figure 13 demonstrates that from Station 7 around to Station 15 the boundary layer edge over the convex wall is almost the same as the streamline. Since the flow accelerates near the start along the convex wall, the streamlines contract and thus are directed toward the wall. In a rotational flow field, the vorticity must be constant along the streamline. Therefore, the boundary layer edge(zero vorticity line theoretically) must follow the contracting streamline. The lack of mass flow into the boundary layer is consistent with the concept that the outer layer of the quasi-laminar flow region is governed by the inviscid rotational mechanism. In this study the boundary layer thickness, $\delta$, was determined as the distance from the wall to the point at which the velocity is 0.99 times the potential flow velocity. As seen in Fig. 6 before, it was not too difficult to decide the approximate value of $\delta$. The vorticity($\Omega_z$) distribution along the streamline over the convex wall is demonstrated in Fig. 14. The vorticity for the curvilinear coordinate is given by,

$$\Omega_z = \left(\frac{1}{1+ky}\frac{\partial V}{\partial x} - \frac{\partial U}{\partial y} - \frac{k}{1+ky}U\right)$$
$$= \left[\left(\frac{1}{1+ky}\frac{\partial V}{\partial x} - \frac{1}{1+ky}\frac{\partial}{\partial y}\right.\right.$$
$$\left.\left.\{(1+ky)U\}\right]\right. \tag{19}$$

Different from the flat wall flow, $\partial U/\partial y$ is negative except very near the wall in the boundary layer along the convex wall. However $\partial(1+ky)U/\partial y$ is positive throughout the boundary layer so that the vorticity is negative. At 45° around the turn the calculated rotational flow results agree well with the experimental data for the region $y/\delta_0 \geq 0.4$ or $y \geq 1.524$ cm, as shown in Fig. 12. Using the streamline coordinate, this value is equivalent to $\psi' = 0.25$ at Station 12(45° around the turn). Figure 14 shows that $\Omega_z$ is approximately constant for $\psi'$ greater than 0.25. This agreement indicates that the calculated

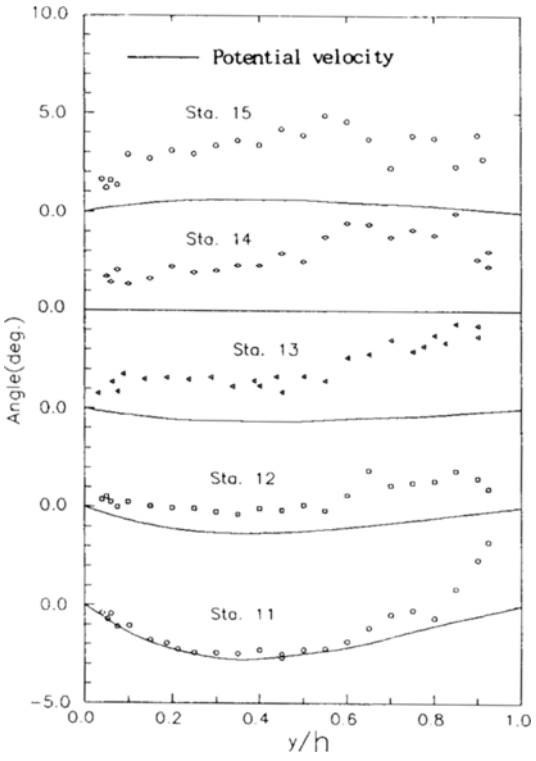


**Fig. 11** Flow angle profiles in the turn

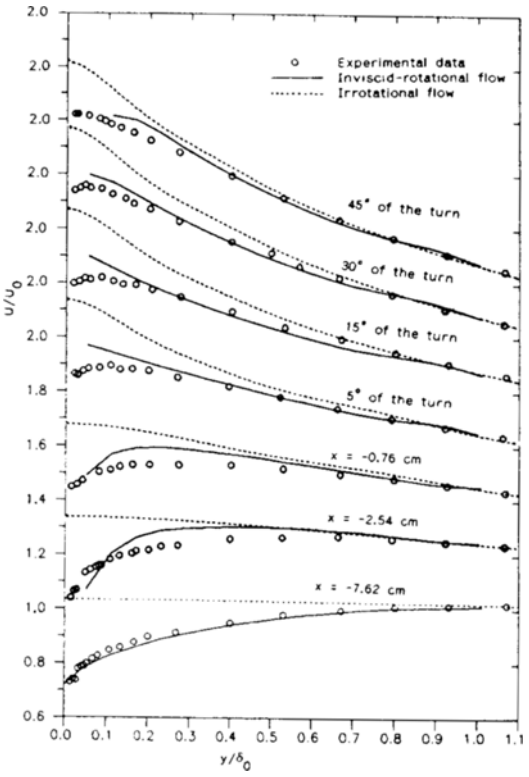


**Fig. 12** Mean velocity profiles near the start of the turn along the inner wall

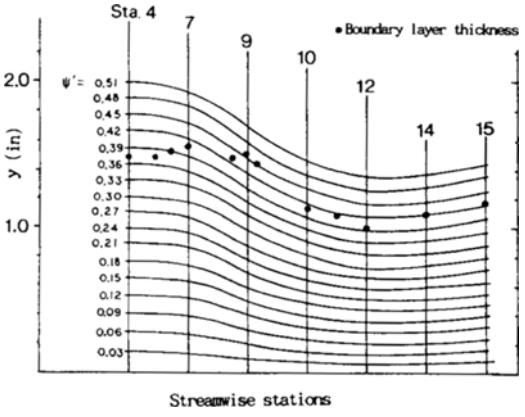


**Fig. 13** Streamlines along the inner wall near the start of the turn

results for rotational flow agree well to the analytical assumption of constant $\Omega_z$ along the streamline. The results also are consistent with the assumption that the flow in this region is inviscid-rotational. Vorticity increases toward the wall and deviations from the constant line are more pronounced very near the wall due to viscous effects.

### 6.3 Mean velocity profiles

Since the static pressure field in the curved section changes rapidly, the mean flow in the turn is greatly influenced by the pressure gradients in both the streamwise and normal directions.

Figure 15 shows an isometric plot of the mean velocity vectors throughout the curved channel. The mean flow in the turn is consistent with the static pressure results. Along the outer concave wall the mean flow velocity decreases first, then stays almost the same between 50° and 130° around the turn and thereafter increases near the turn exit. Along the inner convex wall the mean flow accelerates and then decelerates. At the start and the exit of the turn, the flow shows a high deflection toward the inner wall and the outer wall respectively, showing the inertial effect of the flow in the turn. Beyond the 60° Station the mean velocity decreases and turbulent boundary layer

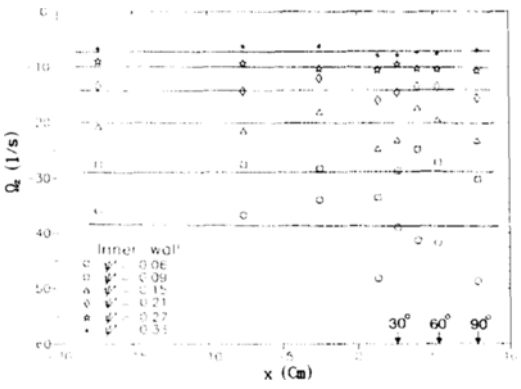


**Fig. 14** Vorticity change along the streamlines

separation eventually occurs on the inner convex wall. Due to the inertial effect and the adverse streamwise pressure gradient increasing in that region, the fluid near the wall becomes to have a lower momentum. The fluid in the boundary layer does not possess sufficient mean kinetic energy and finally separates at approximately 165 ° around the turn. It was observed that the shear layer near the turn exit along the outer concave wall was very thin. This result is due to the fact that both the favorable pressure gradient growing in this region and the higher turbulent mixing due to destabilizing concave curvature contribute to diminish the velocity defect in the shear layer. In addition the inertial effect of the flow causes the higher momentum fluid in the core region to move toward the outer wall near the turn exit, which results in thinning the shear layer down. This thinner shear layer still continued in the straight channel downstream.

If the streamlines are parallel to the wall( $V=0$), the potential velocity profiles $U_p(x, y)$ can be obtained from the vorticity in Eq. (19) since $\Omega_z=0$ in the irrotational flow field.

$$U_p(x, y)=\frac{U_{pw}(x)}{1+k(x)\cdot y} \tag{20}$$

where $U_{pw}$ is the potential velocity at the wall. The displacement thickness for the curved flow is defined,

$$\delta^*=\frac{1}{k}[\exp\{\frac{k}{U_{pw}}\int_0^\delta(U_p-U)dy\}-1] \tag{21}$$

The momentum thickness for the curved flow becomes,

$$\theta=\frac{1}{k}[\{1-\frac{k}{U_{pw}^2}\int_0^\delta U(U_p-U)dy\}^{-1}-1] \tag{22}$$

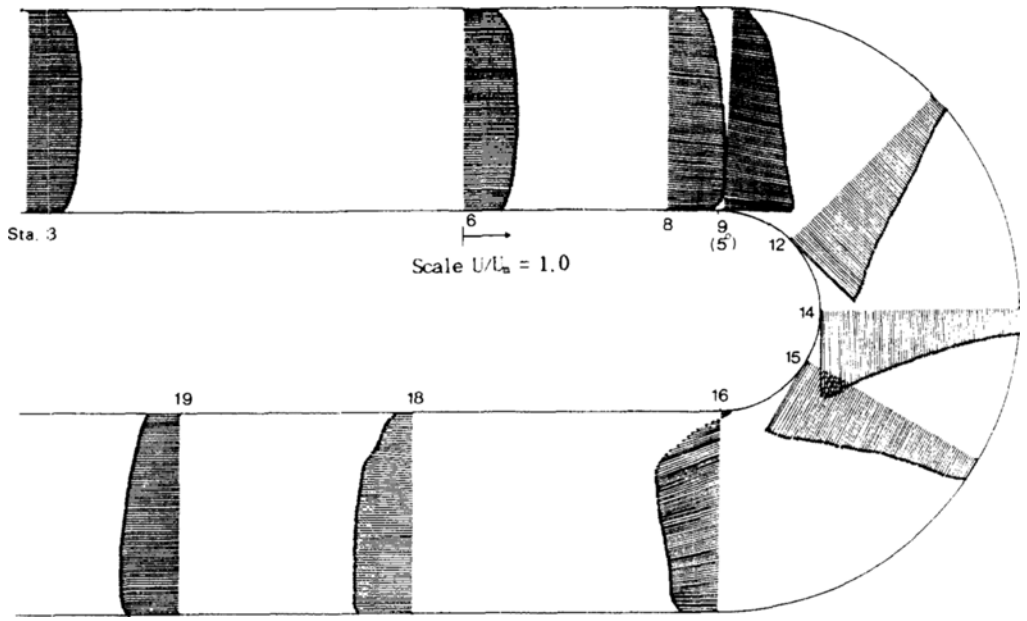


**Fig. 15** Mean velocity profile changes through the turn-around duct

Integral parameters given in Eqs. (21) and (22) are valid only if the potential flow field is represented by Eq. (20). The potential streamlines for the present flow, however, are not parallel to the wall near the start of the turn. Therefore the effective curvature can be introduced in this region so that the streamlines are almost parallel to the wall. The effective curvature, $k_e(x)$, is defined as that $k(x)$ satisfying Eq. (20) when the potential velocity profiles are known. $k_e(x)$ was determined by a least square fit using the calculated potential velocity profiles. $\delta^*$ and $\theta$ in the present study were obtained from Eqs. (21) and (22) using the effective curvature.

The boundary layer growth rate along the convex wall is dependent on the curvature and the pressure gradient effect. For a flow without pressure gradient, Meroney and Bradshaw(1975) reported the growth rate was only half of that of an equivalent plane flow for their curved flow with $\delta/R=0.01$, while So and Mellor's experiment(1972) with $\delta/R=0.08$ showed almost constant $\delta$ along the convex wall. For a pressure gradient flow, Wilken's measurement(1930) shows a decreasing $\delta$ along the convex wall.

Streamwise change of boundary layer parameters are shown in Fig. 16. The boundary layer thickness was slightly greater on the inner wall than the outer wall in the straight section upstream, Fig. 16(a). Accordingly the mean velocity profiles of the oncoming flow were slightly asymmetric between the inner and outer wall with a maximum difference of $\pm 1.5\%$ in the averge velocity at Station 2. A decreasing boundary layer thickness in a quasi-laminar region as shown in Fig. 15(a) agrees well with the previous study(Wilcken, 1930). The boundary layer thickness increases along the outer wall. The boundary layer parameters show that rapid changes are encountered near the onset of curvature. The Clauser shape factor, $G$, is useful to describe the equilibrium state of the boundary layer. $G$ is defined by,

$$G=\sqrt{\frac{2}{C_f}}\left(1-\frac{1}{H}\right) \tag{23}$$

in which H is a shape factor, $H=\delta^*/\theta$. According to Clauser(1956) G has a universal value of 6.8 for a flat wall flow without pressure gradient in the equilibrium state. Figure 16(e) shows that the oncoming flow is influenced by the favorable pressure gradient($G<6.8$). For fully developed curved flow, the velocity defect along the concave wall is smaller than the plane flow so that H is smaller. Exactly the opposite phenomena occur along the convex wall. Figure 16(d) indicates that the flow in the downstream part of the turn

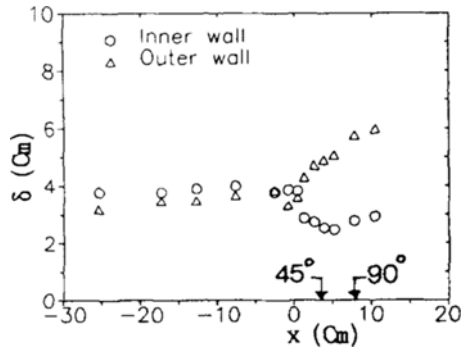


a)Boundary layer thickness

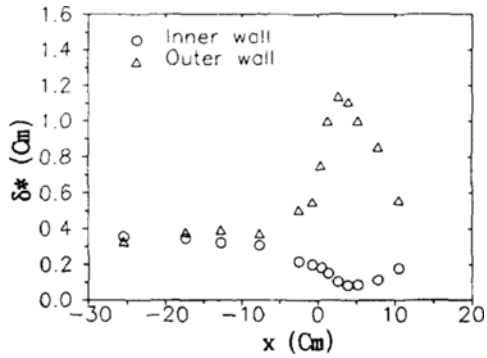


b)Displacement thickness

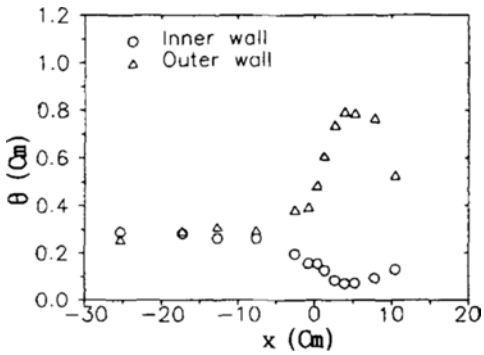


c)Momentum thickness

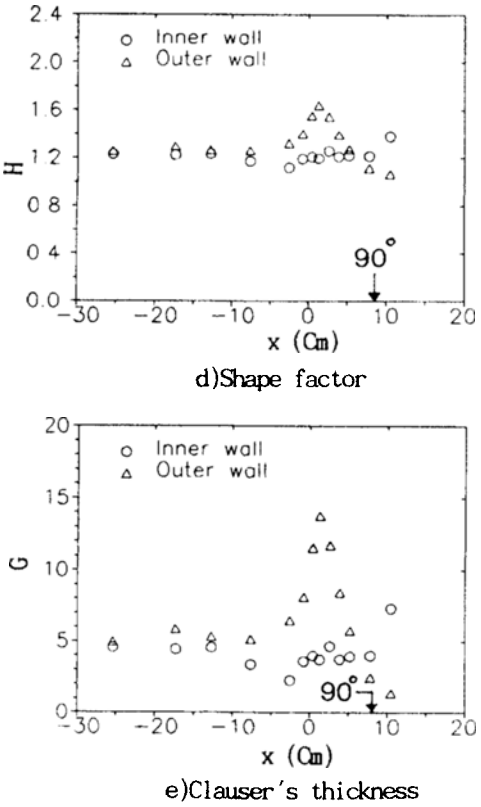


**Fig. 16** Change of boudary layer parameters along the curued duct

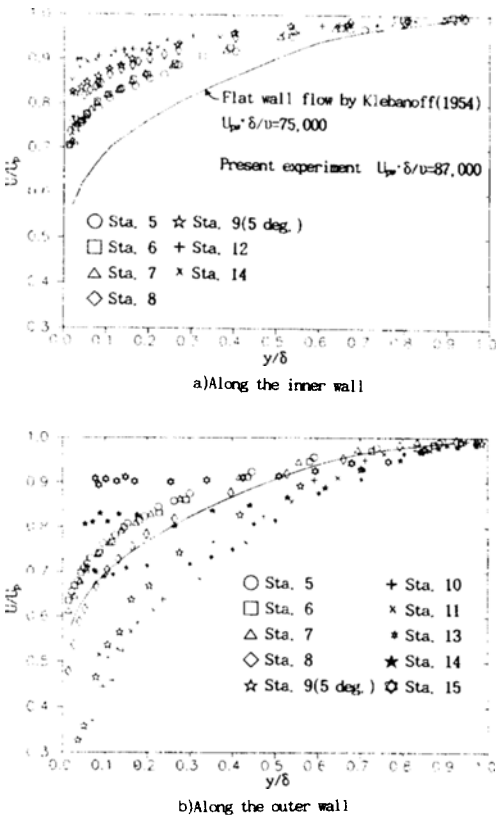


**Fig. 17** Stream development of mean velocity profiles in the turn-aruoud duct

approaches the fully developed curved flow. The straight section downstream and the appearance of separation hinder further development toward the fully developed condition. Before approximately the 90° Station, however, all the boundary layer parameters show that the mean flow is more influenced by the streamwise pressure gradient than by the curvature. The adverse pressure gradient near the start along the outer wall causes H and G to be larger, while the favorable pressure gradient along the inner wall produces smaller values of $H$ and $G$.

Mean velocity profiles normalized by $U_p$ along the curved duct are shown in Fig. 17. For comparison Klebanoff's result for the flat plate flow without pressure gradient is also shown. The flow upstream of the turn(before Station 8), for both the inner and outer walls, is subject to a slightly favorable pressure gradient due to boundary layer growth. The velocity defect in the boundary layer becomes smaller for the accelerated flow and larger for the decelerated flow. For curved flow, the higher momentum fluid moves toward the concave wall and away from the convex wall due to the centrifugal instability. The present flow in the upstream part of the turn(Stations 9 through 14) is opposite to the characteristics of fully developed curved flow. The strong favorable pressure gradient along the convex wall and the adverse pressure gradient along the concave wall surpasses the curvature effect in this region. However the flow in the downstream part of the turn tends to approach the inertial dominated, fully developed conditions. Due to the inertial effect of the flow and concave curvature, the velocity defect in the shear layer becomes smaller along the outer wall(Station 15) as shown in Fig. 17(b).

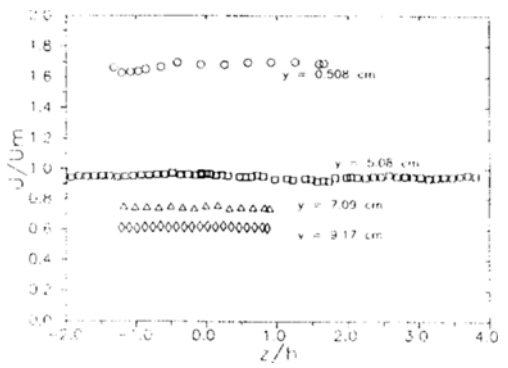


**Fig. 18** Spanwise variations at 90 deg. around the turn

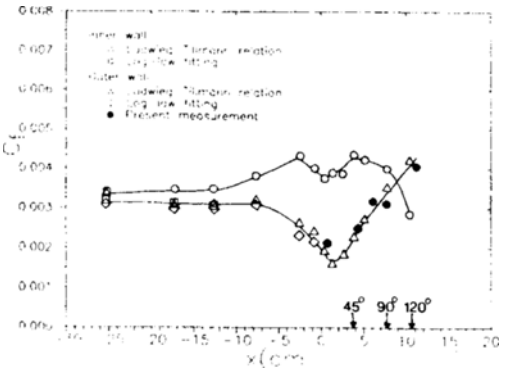


**Fig. 19** Streamwise change of the skin friction coficients

Figure 18 shows the spanwise variation of the mean velocities for different heights at 90° around the turn. Although small variations in the velocity are observed, the flow was nearly two-dimensional across the height. During the start-up of the flow in the facility air bubbles were collected in the upper corners of the outer concave wall. Fortunately, during this short time period, these air bubbles could be used for flow visualization along the outer concave wall. It was observed from flow visualization that Taylor-Görtler vortices do not remain stationary in the present experiment. The longitudinal vortices are highly time dependent, moving rapidly in the spanwise direction, randomly appearing and disappearing. Deviations from two-dimensional flow occur only in the separated region.

### 6.4 Surface shear stresses

Surface shear stress variations with Re on the outer concave wall were measured using a Stanton tube. In this study the Ludwieg-Tillmann relation was employed for the approximate estimation of the surface shear stress where the log-law fitting could not be made.

$$C_f = 0.246(10^{-0.678H} Re_\theta^{-0.268}) \qquad (24)$$

Yamaguchi(1987) and Gibson et al.(1984) reported that the Ludwieg-Tillmann relation for $C_f$ agreed well to their experimental results for the curved boundary layer. The present measurements on the outer wall also shows good agreement with this relation, Fig. 19. The conclusive result for the fully developed curved flow that the skin friction becomes higher on the concave wall and lower on the convex wall compared to the flat wall flow was well documented by the previous investigators.(So et al., 1972; Gillis et al., 1983) The results for 120° around the turn follow the previous results. In the upstream part on the concave wall, $C_f$ decreases, due to the flow deceleration near the start of the turn, and then increases. On the convex wall, however, $C_f$ increases first, due to the flow acceleration, and then decreases.

## 7. Conclusions

The outer layer in the quasi-laminar region is governed by an inviscid-rotational mechanism. Both rotational and irrotational flow calculations predict the flow except very near the wall. However the rotational flow predictions were closer to the measured values. The present turn-around duct flow shows the characteristics of inertial dominated, developing curved flow. Until approximately 90° around the turn, the flow is developing toward the fully developed curved duct flow. Near the start of the turn, the streamwise pressure gradient effect on the flow surpasses the curvature effect. The flow in the downstream part of the turn is rapidly adjusting to the straight section downstream, without reaching an equilibrium state for fully developed curved channel flow. The use of effective wall curvature along which streamlines are assumed to be parallel was found to be reasonable to describe the streamwise mean velocity.

## References


Badrinarayanan, M. A. and Ramjee, A., 1969, "On the Criteria for Reverse Transition in a Two Dimensional Boundary Flow," *J. Fluid Mech.*, Vol. 35, p. 225.

Barlow, R. S. and Johnston, J. P., 1988, "Structure of Turbulent Boundary Layer on a Concave Surface," *J. Fluid Mech.*, Vol. 191, p. 137.

Clauser, F. H., 1956, "Turbulent Boundary Layer," *Advances in Applied Mechanics by H. L. Dryden*, Vol. 4, Academic Press Inc.

Ellis, L. B. and Joubert, P. N., 1974, "Turbulent Shear Flow in a Curved Duct," *J. Fluid Mech.*, Vol. 62, p. 65.

Eskinazi, S. and Yeh, H., 1956, "An Investigation on Fully Developed Turbulent Flows in a Curved Channel," *J. Aero. Sci.*, Vol. 23, p. 23.

Gibson, M. M., Verriopoulos, C. A. and Vlachos, N. S., 1984, "Turbulent Boundary Layer on a Mildly Curved Convex Surface," *Exp. in Fluids*. Vol. 2, p. 17.

Gillis, J. C. and Johnston, J. P., 1983, "Turbulent Boundary Layer Flow and Structure on a Convex Wall and its Redevelopment on a Flat Wall," *J. Fluid Mech.*, Vol. 135, p. 123.

Hunt, I. A. and Joubert, P. N., 1979, "Effects of Small Streamline Curvature on Turbulent Duct Flow," *J. Fluid Mech.*, Vol. 91, p. 633.

Lau, J., 1966, "Recalculation of Incompressible Flow in Two-Dimensional Bends," *Canadian Aeronautics and Space Journal*, Sep.

Launder, B. E., 1963, "The Turbulent Boundary Layer in a Strongly Negative Pressure Gradient," *M.I.T. Gas Turbine Lab. Rep.* No. 71.

Meroney, R. N. and Bradshaw, P., 1975, "Turbulent Boundary Layer Growth over a Longitudinally Curved Surface," *AIAA J.*, Vol. 13, p. 1448.

Monson, D. J., Seegmiller, H. L. and McConnaughey, P. K., 1989, "Comprison of LDV Measurements and Navier-Stokes Solutions in a Two-Dimensional 180-Degree Turn-Around Duct," *27th Aerospace Sciences Meeting*, Jan. 9-12, 1989/Reno, Nevada.

Muck, K. C., Hoffmann, P. H. and Bradshaw, P., 1985, "The Effect of Convex Surface Curvature on Turbulent Boundary Layers," *J. Fluid Mech.*, Vol. 161, p. 347.

Patankar, S. V., 1980, *Numerical Heat Transfer and Fluid Flow*, McGraw Hill Book Company, New York, NY.

Patel, V. C. and Head, M. R., 1968, "Reversion of Turbulent to Laminar Flow," *J. Fluid Mech.*, Vol. 34, p. 371.

Press, W. H., Flannery, B. P., Teukolsky, S. A. and Vettering, W. T., 1986, *Numerical Recipes*, Cambridge University Press, New York, New York.

Ramaprian, B. R. and Shivaprasad, B. G., 1978, "The Structure of Turbulent Boundary Layers Along Mildly Curved Surfaces," *J. Fluid Mech.*, Vol. 85, p. 273.

Rayleigh, J. W. S., 1917, "On the Dynamics of Revolving Fluids," *Pro. of the Roy. Soc. of London*, Vol. 93, Serial A, p. 148.

So, R. M. C. and Mellor, G. L., 1972, "An Experimental Investigation of Turbulent Boundary Layers Along Curved Surfaces," *NASA CR-1940*.

Wattendorf, F. L., 1935, "A Study of the Effect of Curvature on Fully Developed Turbulent Flow," *Pro. Roy. Soc.*, A 148, p. 565.

Wilcken, H., 1930, "Effect of Curved Surfaces on Turbulent Boundary Layers," *NASA TT-F-11421*.

Yamaguchi, H., 1987, "Fundamental Studies on the Control of Turbulent Boundary Layers: Experimental Investigations of the Effect of Convex Curvature on Boundary Layer Characteristics," Nippon Kikai Gakkai Ronbunshu, B-Hen, Vol. 53, N489, May, p. 1505~1510.